Reduction of Torque Ripple method for Small Inductance Brushless DC Motor

S.Rukhaya Taj
M-tech Student Scholar
Department of Electrical & Electronics Engineering,
Godavari Institute of Engineering and Technology, Rajahmundry; East Godavari (Dt); A.P, India.

A. Teja Sri, MTECH
Assistant Professor
Department of Electrical & Electronics Engineering, Godavari Institute of Engineering and Technology, Rajahmundry; East Godavari (Dt); A.P, India

Abstract- In this paper Reduction of Torque Ripples for Small Inductance Brushless DC Motor is presented. In conventional control methods of brushless DC (BLDC) motor drives, back-electromotive force (EMF) is assumed to be in ideal form and the controller injects rectangular phase current commands to produce the desired constant torque. However, real back-EMF waveform might not be exactly trapezoidal because of non-ideality of magnetic material, design considerations and manufacturing limitations. This makes the generated electromagnetic torque contain ripples in its waveform which is not desirable in motor operation performance especially, in sensitive industries. Moreover, commutation states affect the quality of generated torque by producing torque pulsations because of changes of conducting phases.In this paper, an accelerated torque control scheme for small inductance BLDCM with single dc-link current sensor is presented. First, ripple-free electromagnetic torque control is realized in commutation and conduction regions. Second, the disturbance torque is observed and compensated through the improved disturbance torque controller. The performance of the system is evaluated by using MATLAB/SIMULINK software.

Keywords: BLDC Motor, Electromotive force, Torque ripple, Commutation.

I. INTRODUCTION

Electrical motor torque is proportional to the product of magnetic flux and the armature current.Mechanical or load torque is proportional to the product of force and distance. Motor current varies in relation to the amount of load torque applied. When a motor is running in steady state, the armature current is constant, and the electrical torque is equal and opposite of the mechanical torque. When a motor is decelerating, the motor torque is less than the load torque [1]. Conversely, when a motor is accelerating, the motor torque is higher than the load torque. Torque ripple is an effect seen in many electric motor designs, referring to a periodic increase or decrease in output torque as the output shaft rotates. It is measured as the difference in maximum and minimum torque over one complete revolution, generally expressed as a percentage. The smoothness of variable speed drive operation is critical and a viable measure used in the design and development of motion control applications. The torque produced in a brushless DC (BLDC) motor with trapezoidal back electromotive force (BEMF) is constant under ideal conditions. However, in practice, torque ripple appears on the delivered output torque [2]. Some of these ripples result from the natural structure of the motor, while some are related to the motor design parameters. Nevertheless, this torques could be minimized throughout the machine design process. Another source of ripples is associated with the control and drive side of the motor [2]-[4]. Torque pulsations are mainly minimized by two techniques: improved motor designs and improved control schemes. Improved motor design techniques for pulsating torque minimization include skewing, fractional slot winding, short pitch winding, increased number of phases, air-gap windings, adjusting stator slot opening and wedges, and rotor magnetic design through magnet pole arc, width, and positions.

For improved motor control schemes, digital control-based techniques, such as adaptive, preprogrammed current, harmonics injection techniques, estimators and observers, speed loop disturbance rejection, high speed current regulators, commutation torque minimizations and others. The digital control found in many applications in motor drive systems, is used in applications requiring high-speed and precision control.

Sources of Torque Ripples in PMBLDC Motor are as follows:

- **Motor nature:** Ripples associated with motor nature refer to the physical properties and parameters of the motor's manufactured materials. Better selection of materials lead to better performance.
- **Motor structure:** This is associated with the motor's design parameters, such as shape and dimensions. Careful consideration of these parameters leads to good performance design.
- **Motor Control:** Many techniques have been introduced to minimize torque ripples. This paper will highlight the minimization of torque ripples in BLDC motors from the motor control side.

Conventional dc motors are highly efficient and their characteristics make them suitable for use as servomotors. However, their only drawback is that they need a commutator and brushes which are subject to wear and require maintenance [3]. When the functions of

commutator and brushes were implemented by solid-state switches, maintenance-free motors were realized. These motors are now known as brushless dc motors.
Brushless dc motor is most widely used in automotive applications specially on vehicle fuel pumps, due to its high efficiency, small size less maintenance when compare to brush dc motor. Using hall sensor mounted on a rotor, accurate and ripple-free instantaneous torque for position information can be obtained. This results in high cost, poor reliability in vehicle applications [3],[4].To avoid the above mentioned problems, many position sensor less algorithms have been considered as potential solution[5]. The performance of the sensor less drive decreases with the phase shifter in the transient state. Also it is sensitive to the phase delay of the low pass filter (LPF) especially at high speed. Several phase shifters are used in the conventional method to compensate for phase error induced by the LPF of back-EMF are proposed [5]-[7].The position information is found by integrating the back-EMF. This method has an error accumulation problem at low speed [8]. The sensor less control techniques using the phase-locked loop (PLL) and the third-harmonic back-EMF are suggested. The motor commutation drifts away from the desired phase angle due to the conduction of the freewheel diode. Furthermore, the drift angle varies as the motor parameters, speed, and load conditions change.

In addition, the ratio of torque delivered to the size of the motor is higher, making it useful in applications where space and weight are critical factors. Over the years of advanced technology development in power semiconductors, embedded systems, adjustable speed drives (ASDs) control schemes and permanent-magnet brushless electric motor production have contributed for reliable and cost-effective solution for adjustable speed applications [8]-[9]. Household appliances are expected to be one of fastest growing end product market for electronic motor drives (EMDs) over the following next few years. The major appliances include clothes washers, room air-conditioners, refrigerators, vacuum cleaners, freezers, etc. The automotive industry will also see the explosive growth ahead for BLDC type electronically controlled motor system owing to the compact design and high efficiency of BLDC motor [10]. The appliances and devices use the electric motors to convert electrical energy into useful mechanical energy required by the load. Consumers now demand for lower energy costs, better performance, reduced acoustic noise, and more convenience features. In recent years, proposals have been made for new higher energy-efficiency standards for appliance industry, which will be legalized in near future. These energy standards proposals present new challenges for appliance designers.

The control strategies that exhibit a high torque dynamic, one can distinguish the Direct Torque Control (DTC). DTC strategies have been widely implemented in squirrel cage induction machine drives. They allow a direct control of the electromagnetic torque and the stator flux through the application of suitable combinations of the control signals of the inverter switches. Brushless DC (BLDC) motor control strategies, it is quite commonly believed that they are based on the current and torque control approaches. One of the most popular is a generalized harmonic injection to find out optimal current waveforms minimizing the torque ripple [11]-[13].To suppress the modulation ripple caused by phase PWM control method, dc-link buck converter PWM control scheme is employed.In this paper, an accelerated torque control scheme for small inductance BLDCM with single dc-link current sensor is presented. First, ripple-free electromagnetic torque control is realized in commutation and conduction regions. Second, the disturbance torque is observed and compensated through the improved disturbance torque controller.A novel DOB based on acceleration feedback information has been proposed for the force/torque control.

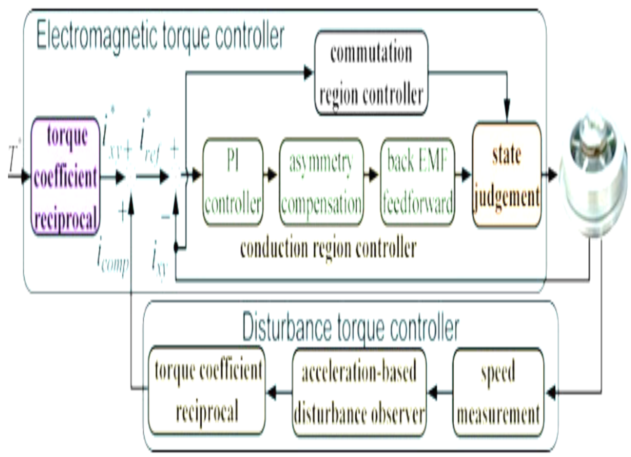

Fig. 1. Accelerated torque control scheme block diagram

II. CONFIGURATION OF THE BLDCM CONTROL SYSTEM

A. System Configuration

The proposed accelerated torque control scheme block diagram is shown in Fig. 1. It mainly consists of an electromagnetic torque controller and a disturbance torque controller. First, ripple-free electromagnetic torque control is implemented through commutation and conduction region current controllers. The commutation region current ripple can be reduced by controlling the outgoing phase, and the conduction region current fluctuations can be regulated through PI control, asymmetry compensation, and back EMF feed forward control. The outputs of commutation and conduction region controllers are used for regulating the three-phase inverter and buck converter respectively. Second, the disturbance torque is estimated by acceleration-based DOB and compensated through the reciprocal of torque coefficient which varies with rotor position. Besides, the estimation process is synchronized with the speed measurement.

B. Drive System Model

p-ISSN: 2348-6848
e-ISSN: 2348-795X
Volume 03 Issue 17
November 2016

The phase current and torque ripples are severe for the small inductance BLDCM when the three-phase inverter is modulated. A torque ripple reduction method has been proposed by adding a buck converter in the front of the three-phase inverter. The buck converter-based BLDCM drive system block diagram is shown in Fig. 2.

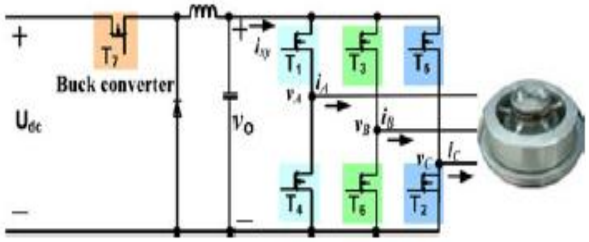

Fig. 2. Buck converter-based BLDCM drive system block diagram.

The BLDCM voltage equation of three phase windings is

$$\begin{bmatrix} v_A \\ v_B \\ v_C \end{bmatrix} = \begin{bmatrix} R_A & 0 & 0 \\ 0 & R_B & 0 \\ 0 & 0 & R_C \end{bmatrix} \begin{bmatrix} i_A \\ i_B \\ i_C \end{bmatrix} + \begin{bmatrix} L_A & 0 & 0 \\ 0 & L_B & 0 \\ 0 & 0 & L_C \end{bmatrix} \frac{d}{dt} \times \begin{bmatrix} i_A \\ i_B \\ i_C \end{bmatrix} + \begin{bmatrix} e_A \\ e_B \\ e_C \end{bmatrix} + \begin{bmatrix} v_{N0} \\ v_{N0} \\ v_{N0} \end{bmatrix} \quad (1)$$

where , , and are the phase-winding terminal-to-ground voltages;, and are the phase-winding currents; , ,and are the line-to-neutral back EMFs; is the neutral point-to-ground voltage; , , and are phase-winding resistances; and , , and are the phase-winding inductances, respectively.

III. ELECTROMAGNETIC TORQUE CONTROL

The electromagnetic torque can be expressed as

$$T_e = \frac{e_A(\theta_e)i_A + e_B(\theta_e)i_B + e_C(\theta_e)i_C}{\omega_m} \quad (2)$$

Where θ is the rotor position, ω is the rotor speed, the subscripts "e" and "m" denote the electrical value and mechanical value, respectively. When a single dc-link current sensor is utilized in the two phase switching mode, the electromagnetic torque in non commutation region can be derived as

$$T_e = \frac{e_x(\theta_e)i_x + e_y(\theta_e)i_y}{\omega_m} = \frac{e_{xy}(\theta_e)i_{xy}}{\omega_m} = k_{xy}(\theta_e)i_{xy} \quad (3)$$

Where the subscripts "x" and "y" denote the conduction phases, is the line-to-line back EMF, ixy is the dc-link current,and is the torque coefficient, i.e., line-to-line back EMF coefficient.

According to (3), the electromagnetic torque control can be divided into two sub problems, each with its own design objective. The first sub problem deals with the estimation of torque coefficient which varies with the rotor position. The second sub problem copes with the dc-link current regulation, which involves the ripple reduction in commutation and conduction regions.

A. Torque Coefficient Acquirement

The torque coefficient can be obtained through line-to-line back EMF coefficient estimation. Due to the imbalance magnetization and installation error of poles, the nonidentity as well as half-wave asymmetry exist in back EMF waveforms. For the coreless stator, magnetic saturation is absent and the effect of winding current to air gap flux can be minimized. It is reasonable to assume that the back EMF is proportional to the rotor speed. Thus, the line-to-line back EMFs can be calculated from rotor speed using shape functions and described as

$$e_{xy}(\theta_e) = f_{xy}(\theta_e) \times \omega_m \quad (4)$$

where is line-to-line back EMF shape function.

The actual back EMF waveforms can be measured offline by constant speed tests. Thus, the back EMF with regard to position can be obtained. To get more accurate back EMF shape functions, a neural network is used for fitting the harmonic information in the waveforms. In fact, for any position, the value of back EMF is relevant to the speed. Consequently, with the shape functions that are predetermined and stored in a look-up table, the back EMF amplitude on each position can be calculated by (4) according to the rotor position and speed feedback information.

Hence, the electromagnetic torque can be calculated according to the line-to-line back EMF shape functions and dc-link current. Dividing one electrical cycle into six sectors. The dc-link current reference can be given as

$$i_{xy}^* = \frac{T^*}{\hat{k}_{xy}(\hat{\theta}_e)} \quad (5)$$

where T * is the reference torque, superscripts "∧" and "∗" denote the estimated and reference values, respectively. In each conduction sector, = .

B. Electromagnetic Torque/DC-Link Current Ripple Reduction

For the advanced performance, emphasis should be placed on the current ripple suppression which will reduces the electromagnetic torque ripple at the same time according to (3). The ripple is mainly composed of commutation ripple and conduction region ripple. There are three main sources of conduction region ripple production in the small inductance BLDCM: modulation ripple, unbalance ripple, and disturbance ripple. Modulation ripple is created by three-phase inverter modulation, which can be reduced by the buck converter PWM control method. Unbalance ripple is induced by the unbalances among three phase windings, especially when single dc-link current sensor is employed. And the disturbance ripple is caused by the motor internal disturbances such as back EMF which acts as disturbance to the current dynamic. This section focuses on solving the problem of the current ripple for the small inductance BLDCM with a single current sensor.

1) Commutation Ripple Reduction: As the commutation duration is very short for the small inductance motor, conventional commutation control schemes will not work, and may result in negative influence. Accordingly, it is necessary to improve the commutation region current performance for the small inductance.

International Journal of Research
International Journal of Research
Available at https://edupediapublications.org/journals
p-ISSN: 2348-6848
e-ISSN: 2348-795X
Volume 03 Issue 17
November 2016

According to (1), the neutral point-to-ground voltage can be derived as BLDCM.

$$v_{N0} = \frac{1}{3}(v_A + v_B + v_C - e_A - e_B - e_C) \tag{6}$$

Using phase A as the non commutation phase, phase B as the outgoing phase, and phase C as the incoming phase. According to the voltage equations (1) and (6), phase currents are determined.

$$\begin{cases} i_A = \left(i_{AB} - \frac{V_{A0}}{R_A}\right)\exp\left(-\frac{R_A}{L_A}t\right) + \frac{V_{A0}}{R_A} \\ i_B = \left(-i_{AB} - \frac{V_{B0}}{R_B}\right)\exp\left(-\frac{R_B}{L_B}t\right) + \frac{V_{B0}}{R_B} \\ i_C = \left(-\frac{V_{C0}}{R_C}\right)\exp\left(-\frac{R_C}{L_C}t\right) + \frac{V_{C0}}{R_C} \end{cases} \tag{7}$$

where is the dc-link current before commutation, and the winding impedance voltages V_{A0}, V_{B0}, and V_{C0} can be expressed as

$$\begin{cases} V_{A0} = \frac{v_o - 2e_A + e_B + e_C}{3} \\ V_{B0} = \frac{v_o - 2e_B + e_A + e_C}{3} \\ V_{C0} = \frac{-2v_o - 2e_C + e_A + e_B}{3} \end{cases} \tag{8}$$

where is the buck converter output voltage.

The falling time of outgoing phase and rising time of incoming phase can be calculated as

$$t_{B\_\mathrm{fall}} = -\frac{L_B}{R_B}\ln\left(\frac{V_{B0}}{i_{AB}R_B + V_{B0}}\right) \tag{9}$$

$$t_{C\_\mathrm{rise}} = -\frac{L_C}{R_C}\ln\left(1 + \frac{i_{AB}R_C}{V_{C0}}\right) \tag{10}$$

It can be derived that   when the buck converter output voltage is certain. The decrease rate of , which is associated with the conduction of the free-wheel diode, will be so high that the increase rate of   cannot be increased sufficiently, and the current dips during commutation.

In order to maintain current constant during commutation, the switching OFF of phase B can be delayed and the motor can be operated in the three-phase switching mode. Generally speaking, in the buck converter-based drive system the output of the current controller is employed to regulate the buck converter, while the three-phase inverter is just used for phase conversion. Accordingly, an additional current controller is required to control the outgoing phase during commutation. And the control and modulation frequencies should be set extremely high to avoid the ripple caused by three-phase inverter modulation during commutation. Then, the phase currents will be controllable throughout the commutation period. The time which is taken for iB to decay to zero can be extended by controlling the switch of phase B with PWM as shown in Fig. 3. In the two-phase switching mode, the dc-link current sensor cannot reflect the real phase current during commutation.

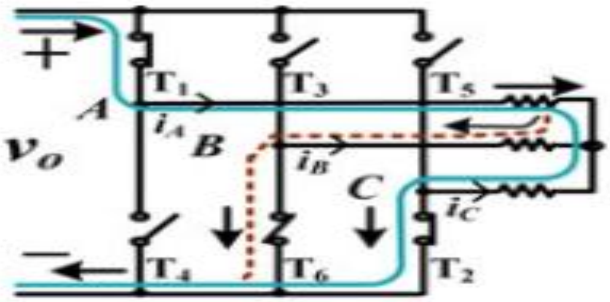

(a)

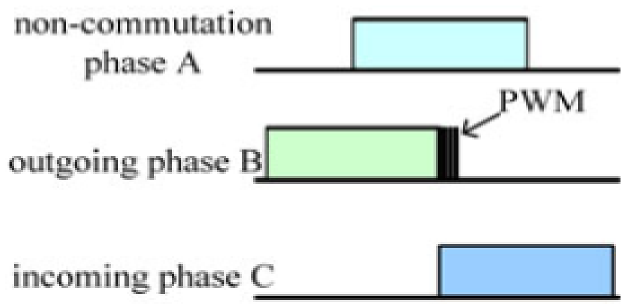

(b)

Fig. 3. Current paths and switching states during commutation control. (a) Current paths in the three-phase inverter. (Solid line represents the current in continuous conduction mode, and the dotted line represents the current modulated by PWM). (b) Switching states of the three-phase inverter.

current during commutation. But it is reasonable to assume that $i_A = -(i_B + i_C) = i_{xy}$ in the three-phase switching mode, and eB (θe) ≈ eC (θe) as the commutation process is very short for a small inductance motor. Therefore, the electromagnetic torque in three-phase switching mode can be expressed as (4) for simplicity. Assuming that the duty ratio of switch $T6$ is D to minimize the commutation ripple, the phase voltage equations during the commutation period can be described as

$$\begin{cases} v_A = v_o = R_A i_A + L_A \frac{di_A}{dt} + e_A + v_{N0} \\ v_B = (1-S)\cdot v_o = R_B i_B + L_B \frac{di_B}{dt} + e_B + v_{N0} \\ v_C = 0 = R_C i_C + L_C \frac{di_C}{dt} + e_C + v_{N0} \end{cases} \tag{11}$$

where S is the switching function. $S = 1$ denotes switching ON and $S = 0$ denotes switching OFF. The neutral point-to-ground voltage can be derived as

$$v_{N0} = \frac{(2-S)v_o - e_A - e_B - e_C}{3} \tag{12}$$

Assuming that the PWM carrier cycle is TPWM , so S remains 1 during DTPWM and 0 during (1 - D)TPWM. Using the state space averaging technique, equation (13) can be expressed as

$$v_{N0} = \frac{(2-D)v_o - e_A - e_B - e_C}{3} \tag{13}$$

Substituting (14) into (12), it is found that the phase currents can be described as (8) unchangeably. While the winding impedance voltages equation (9) is updated as

International Journal of Research
Available at https://edupediapublications.org/journals
p-ISSN: 2348-6848
e-ISSN: 2348-795X
Volume 03 Issue 17
November 2016

$$\begin{cases} V_{A0} = \dfrac{(1+D)v_o - 2e_A + e_B + e_C}{3} \\ V_{B0} = \dfrac{(1-2D)v_o - 2e_B + e_A + e_C}{3} \\ V_{C0} = \dfrac{(D-2)v_o - 2e_C + e_A + e_B}{3} \end{cases} \tag{14}$$

Expanding exp(-*Rxt/Lx*) in (8) through the Taylor series, its quadratic term or more is neglected. So exp(-*Rxt/Lx*) ≈*1−Rxt/Lx.* Substituting it into (7)

$$\begin{cases} i_A = \left(i_{AB} - \dfrac{V_{A0}}{R_A}\right)\left(1 - \dfrac{R_A}{L_A}t\right) + \dfrac{V_{A0}}{R_A} \\ i_B = \left(-i_{AB} - \dfrac{V_{B0}}{R_B}\right)\left(1 - \dfrac{R_B}{L_B}t\right) + \dfrac{V_{B0}}{R_B} \\ i_C = \left(-\dfrac{V_{C0}}{R_C}\right)\left(1 - \dfrac{R_C}{L_C}t\right) + \dfrac{V_{C0}}{R_C}. \end{cases} \tag{15}$$

The falling time of outgoing phase and rising time of incoming phase can be calculated as

$$\begin{cases} t_{B\_\text{fall}} = \dfrac{L_B i_{AB}}{R_B i_{AB} + V_{B0}} \\ t_{C\_\text{rise}} = -\dfrac{L_C i_{AB}}{V_{C0}}. \end{cases} \tag{16}$$

So, the duty ratio D for minimizing the commutation ripple can be solved as

$$D = \frac{2e_{AB} + 3R_B i_{AB}}{v_o} - 1 \tag{17}$$

As the winding inductance is very small which can be neglected, it is reasonable to assume that $v_o \approx e_{AB} + 2R_B i_{AB}$ Hence, $1 \leq (2e_{AB} + 3R_B i_{AB})/vo \leq 2$.

Since the line-to-line back EMF can be calculated according to the shape functions, the duty ratio can be expressed as

$$D = \frac{2\hat{e}_{xy} + 3R_y i_{xy}}{v_o} - 1 \tag{18}$$

Consequently, the commutation ripple, which would otherwise result from the uncontrollable conduction of free-wheel diodes with the conventional two-phase switching mode during commutation, is minimized.

2) Conduction Region Ripple Reduction:

The conventional ripple control approaches concentrate on commutation ripple reduction, which can work well with the general system. However, for the system with unbalanced windings and single dc link current sensor, it is far from enough. This part focuses on suppressing the conduction region ripples that are caused by unbalanced windings and the back EMF disturbance. The configuration of current PI controller supposing that the disturbance voltage *exy* is fully compensated by a stable back EMF estimator combined with the feed forward control, the transfer function of the current PI controller is greatly simplified.

$$G_c(s) = \frac{i_{xy}(s)}{i^*_{xy}(s)} = \frac{K_{pc}s + K_{ic}}{L_{xy}s^2 + (K_{pc}+R_{xy})s + K_{ic}} \tag{19}$$

where *Kpc* and *Kic* are the PI gains, *Rxy* and *Lxy* are line winding resistance and inductance, respectively. If a desired current loop bandwidth *ωc* is defined, then the controller gains are selected as *Kpc*= *ωcLxy* and *Kic*= *ωcRxy* , respectively. To overcome the unbalanced windings problem, an asymmetry compensation method is proposed. As the winding inductance is very small which can be neglected, the accurate knowledge of the motor resistance *Rxy* is required in the proposed asymmetry compensation method. Assuming that phase *x* and phase *y* are conducted in the two-phase switching mode, according to the phase voltage equation (2), the three-phase inverter terminal voltage equation can be expressed as

$$v_o = R_{xy} i_{xy} + L_{xy}\frac{di_{xy}}{dt} + e_{xy} \tag{20}$$

The three-phase inverter terminal voltage equation (22) can be represented by (23) in z-domain with zero-order-hold conversion:

$$i_{xy}(z) = \frac{\beta(v_o(z) - e_{xy}(z))}{z - \alpha} \tag{21}$$

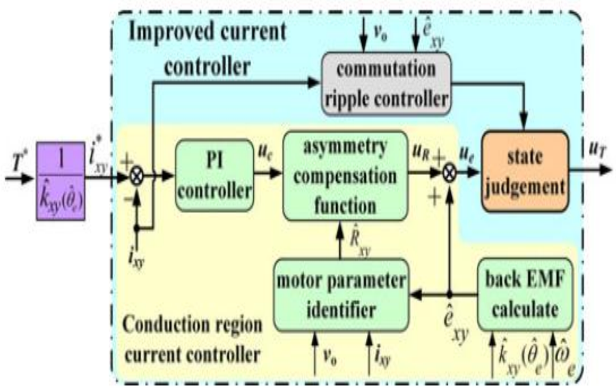

Fig. 5. Improved electromagnetic torque controller block diagram

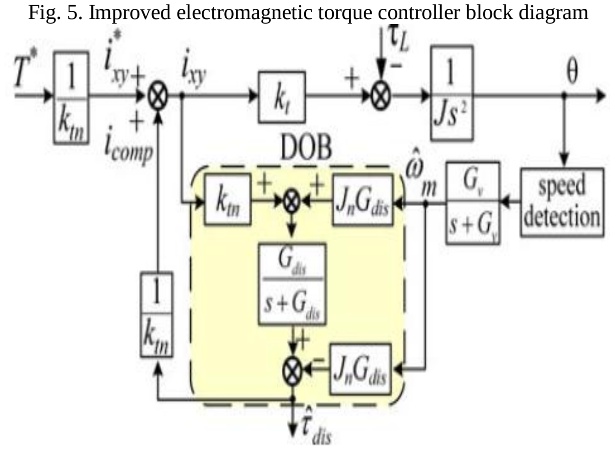

Fig. 6. DOB estimation and compensation block diagram.

Furthermore, the disturbance voltage can be compensated through feed forward control. Line-to-line back EMF amplitude on each position can be calculated by (5) according to the predetermined line-to-line back EMF coefficient and rotor position speed feedback information. Consequently, the output of conduction region current controller can be given as

$$u_e = f(\hat{R}_{xy}) \times u_c + \hat{e}_{xy} \qquad (22)$$

Therefore, the improved electromagnetic torque performance can be obtained with the help of torque coefficient estimation and dc-link current control. The configuration of the electromagnetic torque controller is depicted in Fig. 5.

IV. DISTURBANCE TORQUE SUPPRESSION

A. Acceleration-Based DOB

From (1), it is found that the disturbance toque can be calculated from the difference between electromagnetic torque and accelerated torque. The accelerated torque is proportional to the acceleration. However, in practice, it is difficult to detect the acceleration directly. Thus, the literature proposed a newly designed DOB by which the disturbance toque can be calculated from the rotor speed and the reference current, as shown in Fig. 6. Here, dis is estimated disturbance torque. *G*dis and *Gv* are the DOB and speed estimation LPF cutoff frequencies, respectively. kt is the torque constant, and J is the motor inertia, respectively. Subscripts "n" and "comp" denote nominal and compensation values, respectively

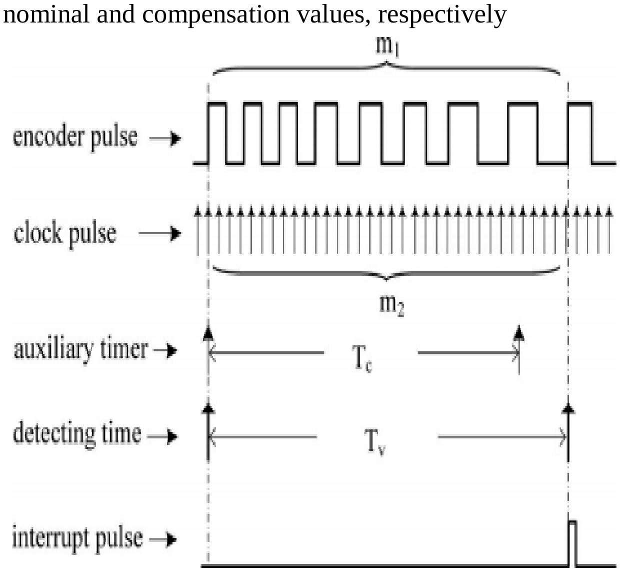

Fig. 7. Speed detection updates timing chart

In order to reduce the noise amplified by the calculation, disturbance torque is estimated through the LPF. Then, the calculated disturbance torque dis is given by (23). In Fig. 6, the total reference current is the sum of the reference current *ixy* and the compensation current *i*comp which cancels out the total disturbance effects.

The DOB is based on the acceleration ˆ*ωms* that derived from the optical encoder output. In other words, the control system has acceleration feedback in essence. It is worth noting that the DOB developed here does not contain a pure derivative as shown in Fig. 6, although it is a common problem in the realization of most DOBs. Note, factors that influence the accuracy of disturbance torque estimation include torque coefficient acquirement, dc-link current tracking performance, rotor speed estimation, and LPF design.

$$\left.\begin{aligned}
\hat{\tau}_{\text{dis}} &= \frac{G_{\text{dis}}}{s+G_{\text{dis}}}(k_{tn}(i^*_{xy}+i_{\text{comp}}) - J_n\hat{\omega}_m s) \\
&= \frac{G_{\text{dis}}}{s+G_{\text{dis}}}(k_{tn}(i^*_{xy}+i_{\text{comp}}) + J_n G_{\text{dis}}\hat{\omega}_m) - J_n G_{\text{dis}}\hat{\omega}_m \\
&= \frac{G_{\text{dis}}}{s+G'_{\text{dis}}}\tau_L \left(G'_{\text{dis}} = \frac{k_t}{k_{tn}} G_{\text{dis}}\right) \\
i_{\text{comp}} &= \frac{\hat{\tau}_{\text{dis}}}{k_{tn}}
\end{aligned}\right\} \qquad (23)$$

B. Rotor Speed Estimation

Since the acceleration-based DOB strongly requires accurate speed measurement, the encoder signal is measured by the M/T method and the principle is shown in Fig. 7. Here,*m*1 and*m*2 are the numbers of encoder pulses and clock pulses during detecting time *Tv* . *Tc* is the prescribed minimum measurement time whose width is fixed. This method has high precision since the starting and ending of detecting time *Tv* are all synchronized with the timing of encoder pulses edges. Besides, the disturbance observation process is also synchronized with the pulsesedges.

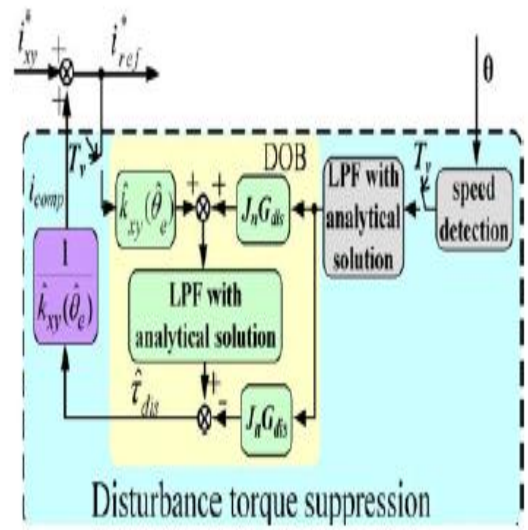

Fig. 8. Improved disturbance torque suppression block diagram.

Accordingly, the speed measurement accuracy can be maximized through the simple principle. The estimated speed is expressed as

$$\hat{\omega}_m = \frac{2\pi f_c m_1}{P m_2} \qquad (24)$$

where P denotes the encoder pulses number per rotation and fc is the frequency of clock pulse, respectively.
The analytical solution of an LPF which is given by

$$\widehat{\omega}_{m(k)} = (1 - \exp^{-G_v T_v})(\hat{\omega}_{m(k)} - \widehat{\omega}_{m(k-1)}) + \widehat{\omega}_{m(k-1)} \qquad (25)$$

The analytical solution provides a much accurate filtering since the digitized LPF is the approximation of an analog LPF. Therefore, the improved disturbance torque suppression performance is achieved and its block diagram is depicted in Fig. 8.

V.MATLAB/SIMULINK RESULTS

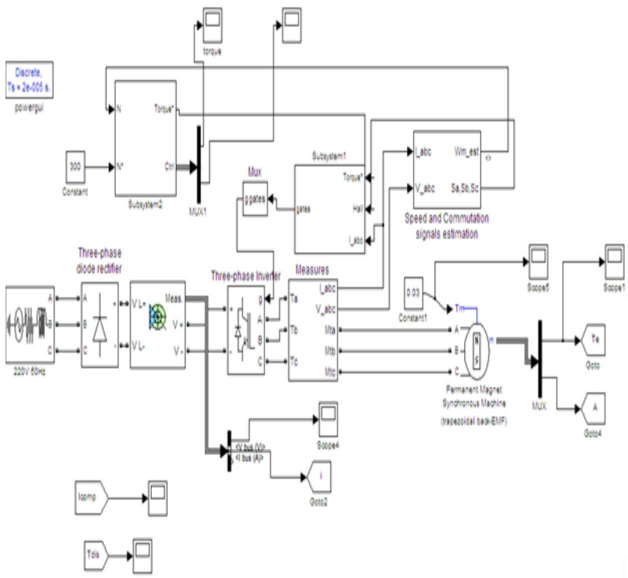

Fig:9 Inductance Brushless DC Motor with Accelerated torque control scheme

Accelerated torque controller:Sudden DC-link drop:

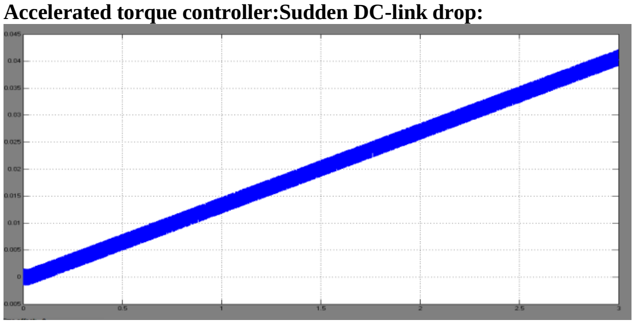

Fig:10 accelerated torque

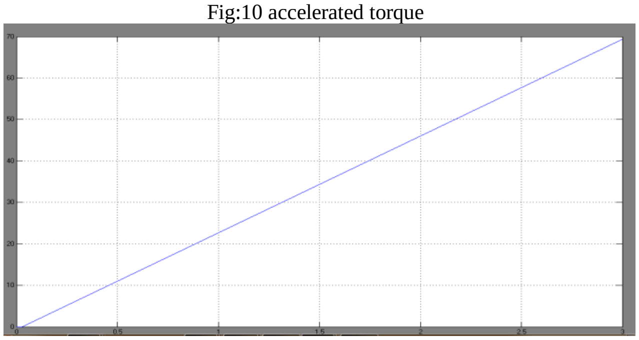

Fig:11 rotor speed.

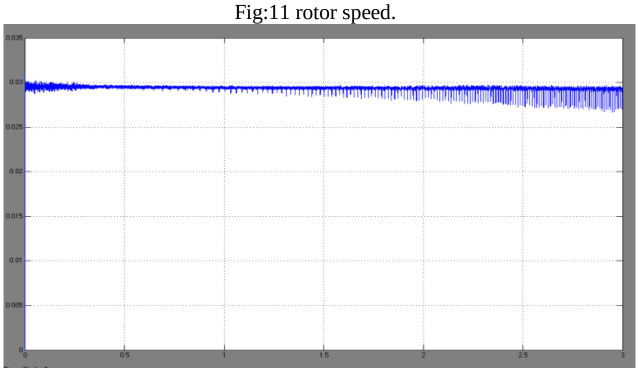

Fig:12 electromagnetic torque.

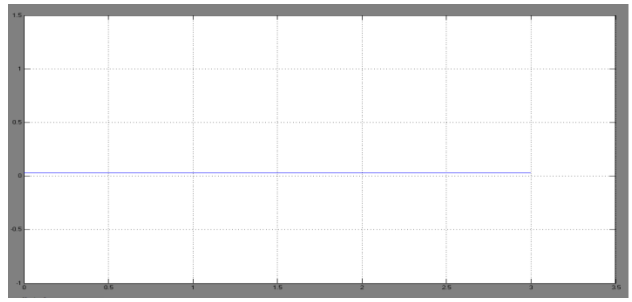

Fig:13 reference torque.

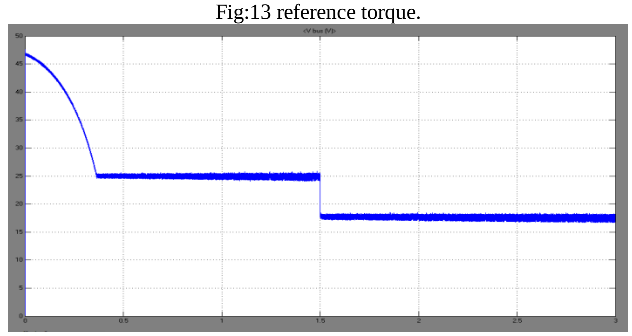

Fig:14 Inverter bus voltage.

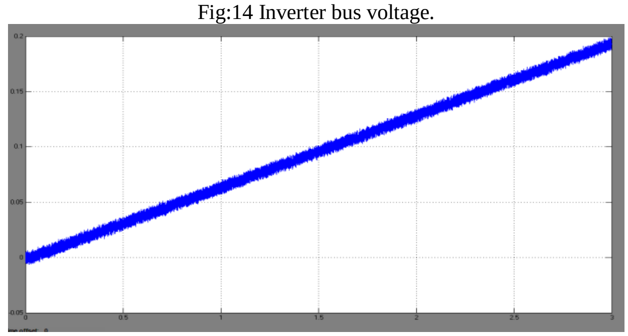

Fig:15 compensation current.

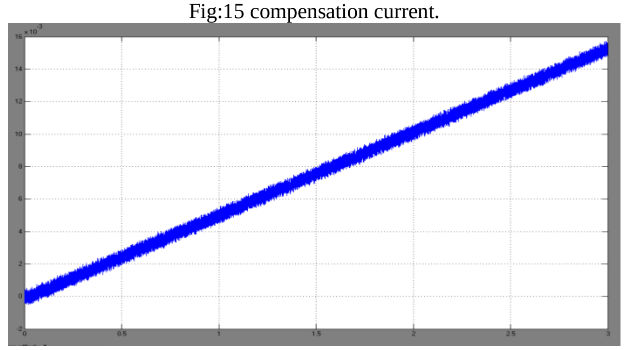

Fig:16 Estimated disturbance torque.

Sudden reference torque change:

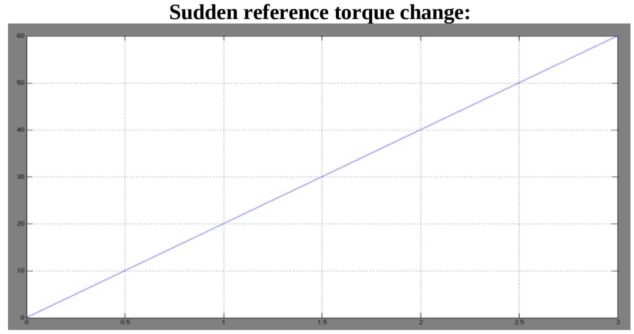

Fig:17 sudden reference torque change.

International Journal of Research
Available at https://edupediapublications.org/journals
p-ISSN: 2348-6848
e-ISSN: 2348-795X
Volume 03 Issue 17
November 2016

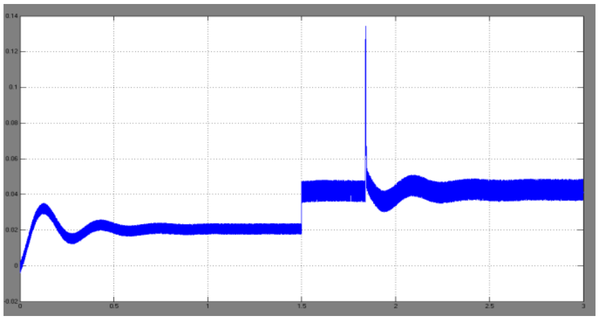
Fig:18 accelerated torque of accelerated torque controller.

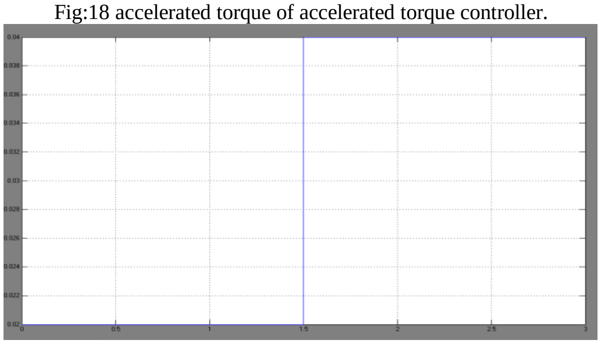
Fig:19 reference torque of accelerated torque controller.

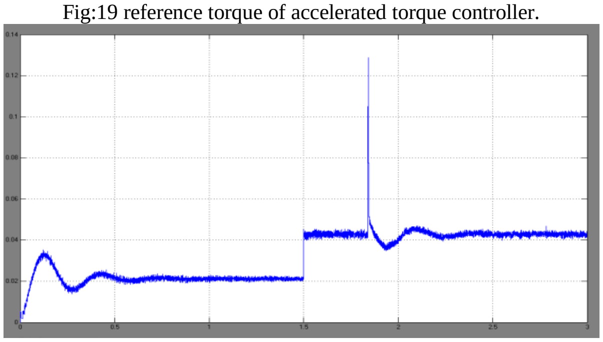
Fig:20 electromagnetic torque of accelerated torque controller.

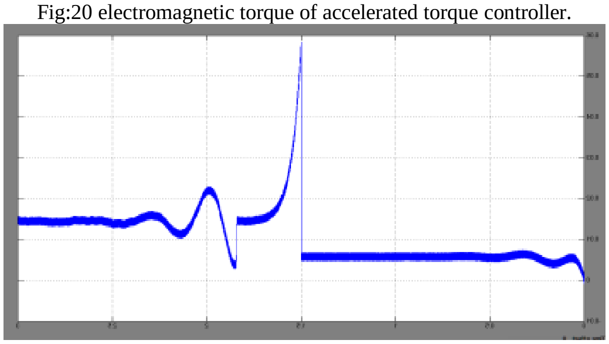
Fig:21 Estimated disturbance torque.

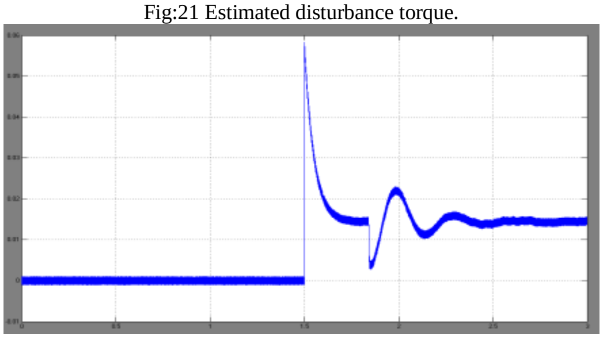
Fig:22 compensation current.

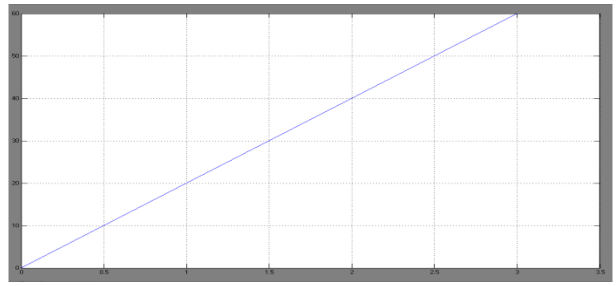
Fig:23 rotor speed.

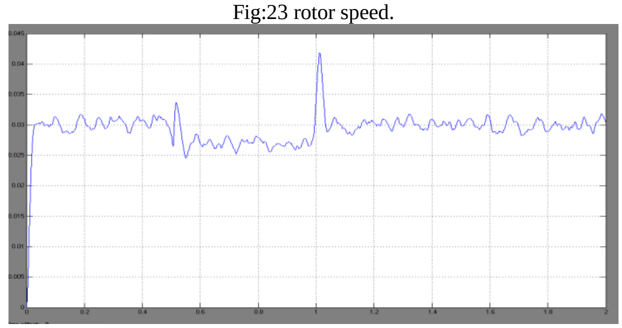
Fig.24. Waveforms of the accelerated torque controller with disturbance torque suppression. (a) Estimated electromagnetic torque.

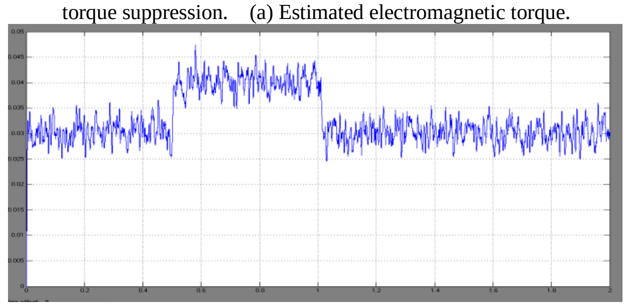
Fig.24. Waveforms of the accelerated torque controller with disturbance torque suppression. (b) Accelerated torque.

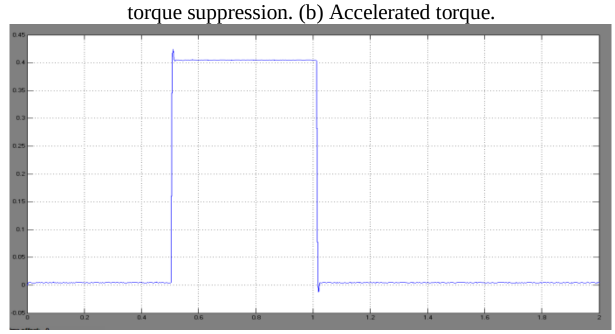
Fig:24(c) Estimated disturbance torque.

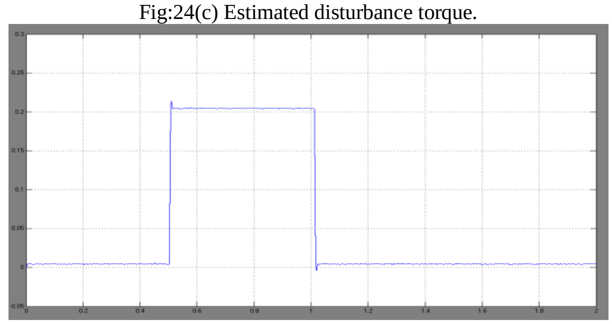
Fig:24(d) Compensation current.

Fig.24. Waveforms of the accelerated torque controller with disturbance torque suppression. (c) Estimated disturbance torque and (d)compensation current.

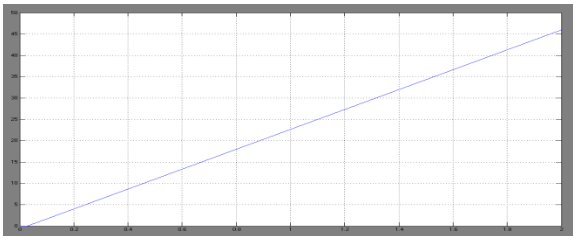

Fig.24. Waveforms of the accelerated torque controller with disturbance torque suppression. (e) Rotor speed.

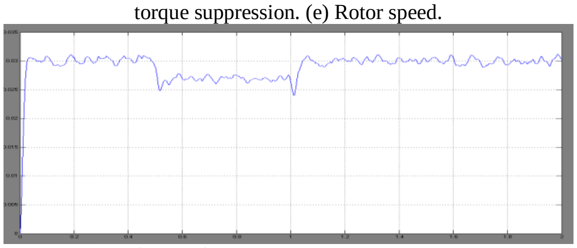

Fig.25. Waveforms of the accelerated torque controller without disturbance torque suppression. (a) Estimated electromagnetic torque.

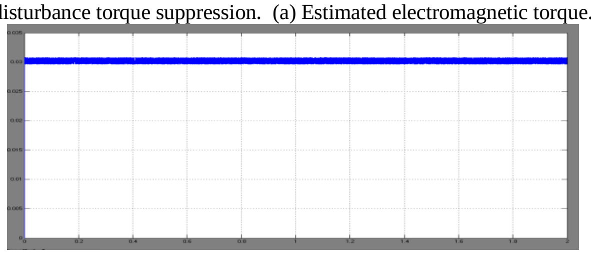

Fig.25. Waveforms of the accelerated torque controller without disturbance torque suppression. (b) Accelerated torque.

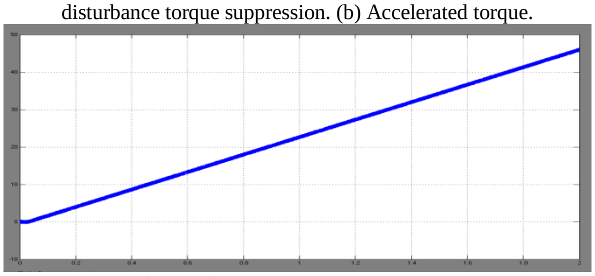

Fig.25. Waveforms of the accelerated torque controller without disturbance torque suppression. (c) Rotor speed.

Sudden reference speed change:

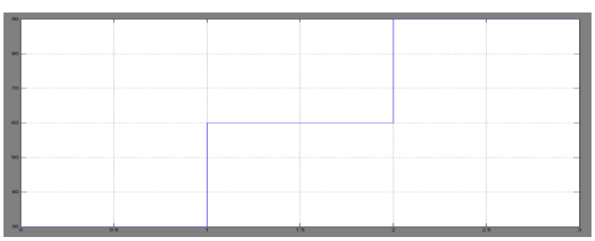

Fig: 26 Sudden reference speed change.

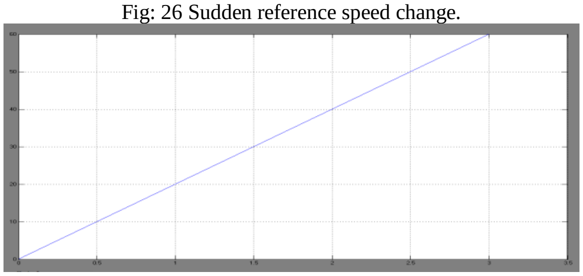

Fig:27 Rotor speed.

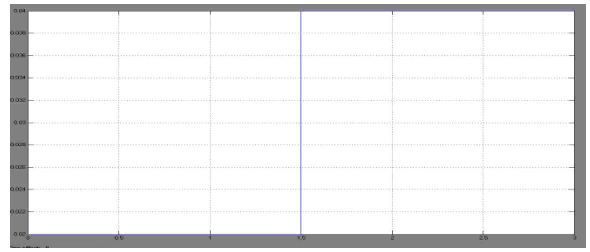

Fig:28 Reference torque.

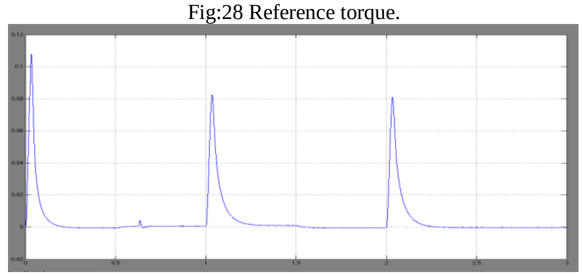

Fig:29 Estimated disturbance torque when sudden reference speed change.

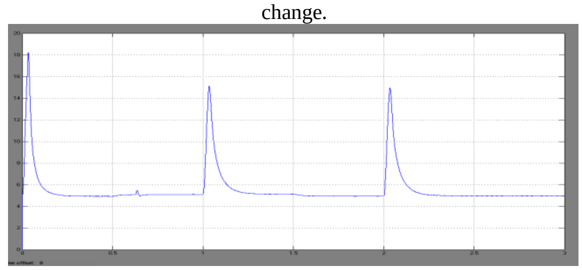

Fig:30 compensation current when sudden reference speed change.

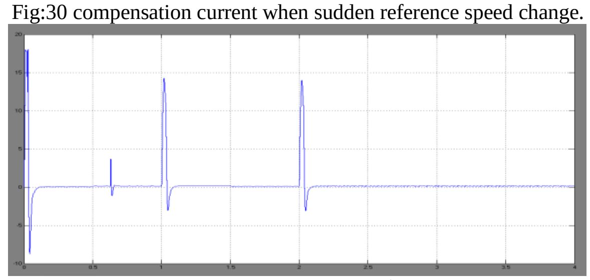

Fig:31 Accelerated torque when sudden reference speed change.

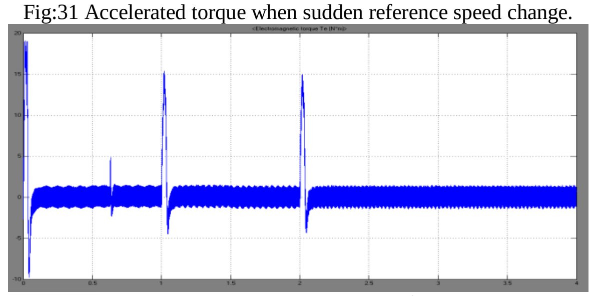

Fig:32 Electromagnetic torque when sudden reference speed change.

When the accelerated torque controller is designed without disturbance torque suppression, the electromagnetic torque can be accurately controlled through the improved current controller, as shown in Fig. 24(a). Fig. 25(b), it is found that the accelerated torque fluctuation decreases by 70% compared with the counterpart of accelerated torque controller without disturbance suppression.

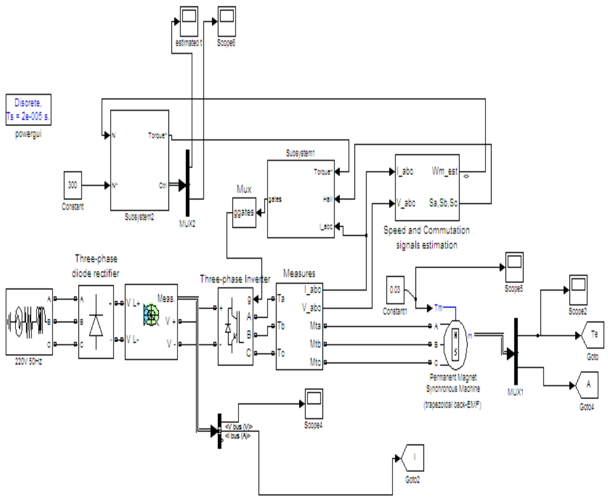

Fig:33 Inductance Brushless DC Motor withElectromagnetic torque control scheme.

Case I: Sudden DC-link drop:

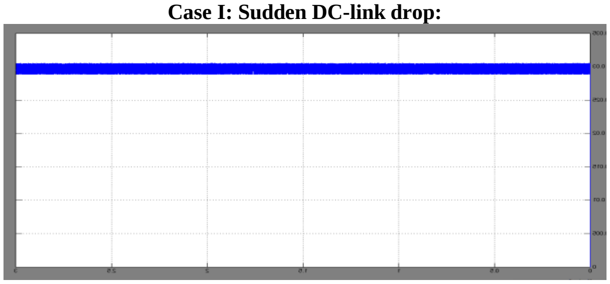

Fig: 34 (a) accelerated torque.

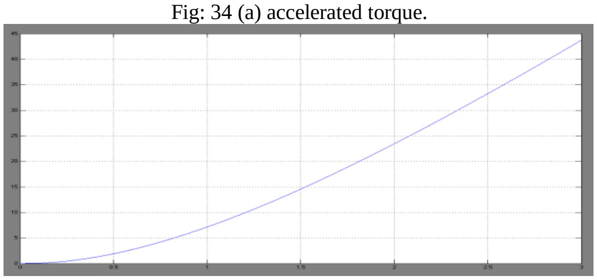

Fig:34(b) Rotor speed.

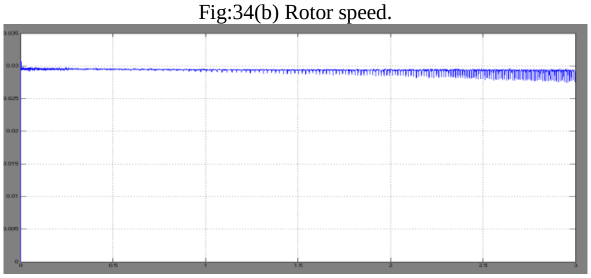

Fig:34(c) Electromagnetic torque.

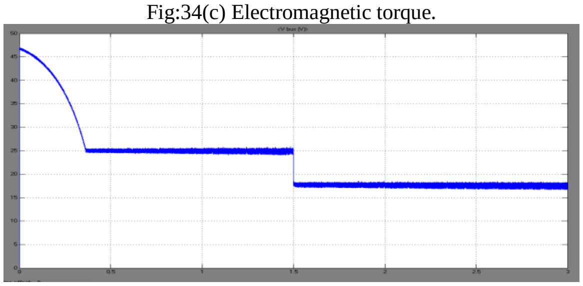

Fig:34(d) disturbance torque

Case II: Sudden reference torque change:

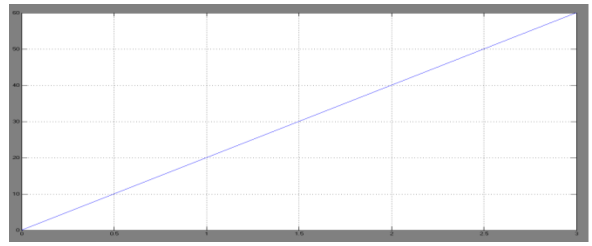

Fig:35(a) Sudden reference torque change.

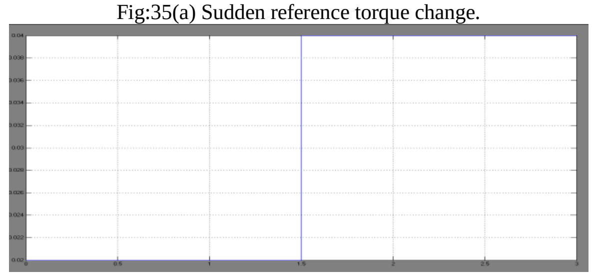

Fig:35(b) Reference torque.

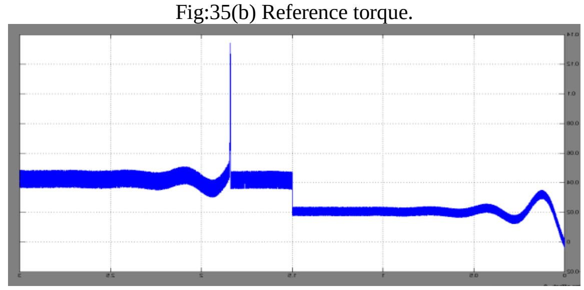

Fig:35(c) Accelerated torque.

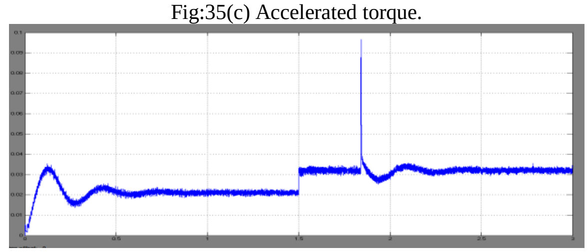

Fig:35(d) Electromagnetic torque.

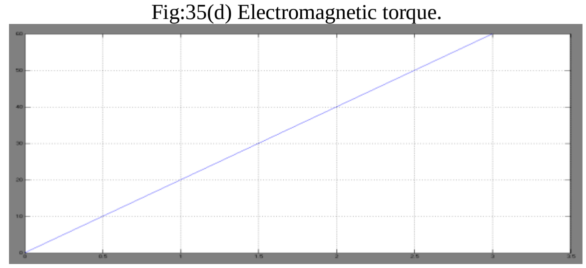

Fig:35(e) Rotor speed.

Fig.35. Waveforms of the accelerated torque controller and electromagnetic torque controller.

Case III: Sudden reference speed change:

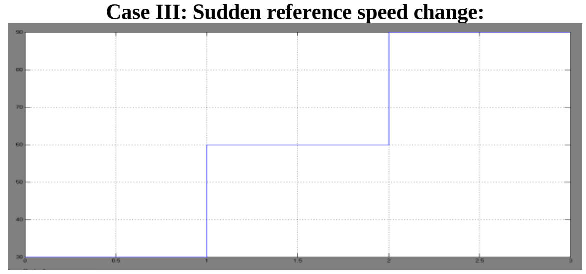

Fig:36(a) Sudden reference speed change.

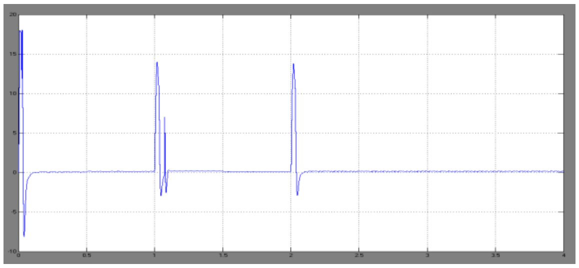
Fig:36(b) Acceleration torque.

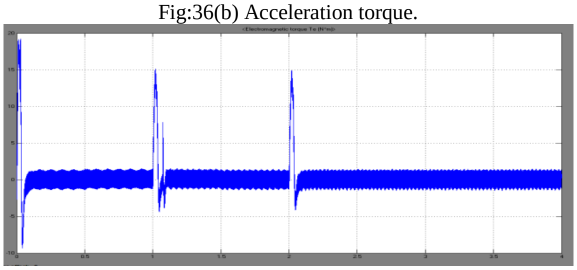
Fig:36(c) electromagnetic torque.

The accelerated torque control system performance is presented in fig 35. The electromagnetic torque control system performance is reported in three ways such as Sudden dc-link drop,Sudden reference torque change, Sudden reference speed change.

VI. CONCLUSION

In this paper Torque ripples can be reduced for small inductance brushless DC motor by improving the electromagnetic torque control and disturbance torque suppression.Electromagnetic torque improvement is achieved by reducing current ripple in the commutation and conduction regions. The commutation region ripple, which would otherwise result from the uncontrollable conduction of free-wheel diodes with the conventional two-phase switching mode during commutation, is minimized by overlapping commutation control and optimizing the duty ratio of the active controller. In the conduction region, the ripple caused by three-phase inverter modulation is suppressed by the buck converter PWM control method.EMF is compensated by feed forward control.

The disturbance torque is suppressed by the disturbance torque controller which has been improved from four aspects. 1) The accurate torque coefficient for disturbance compensation is obtained through line-to-line back EMF coefficient estimation whose harmonic information is fitted by neural network. 2) The improved dc-link current performance is achieved through commutation and conduction region current controllers. 3) The acceleration-based DOB is employed to estimate the disturbance torque, which is a feasible solution for compliant motion in an unknown environment. 4) Accurate disturbance torque and speed estimations have been obtained by the synchronized speed measurement and digitized LPF. Finally ripples of the Torque are reduced in the BLDC motor.

REFERENCES

[1] S.Anishraj, B.Thamizhkani,"Direct Torque Control for Reduction of Torque Ripple During Commutations Using B4-Inverter"International Journal of Revolution in Electrical and Electronic Engineering (IJREEE),Volume 2 Issue 1Mar 2015.
[2] Sharmila Kumari.M, Sumathi.V, Vivekanandan S, Shobana S,"Performance Improvement of BLDC Motor Using Fuzzy Logic Controller"International Journal of Scientific & Engineering Research, Volume 5, Issue 4, April-2014.
[3] P. Deepakumari, Dr. P. Arockia Jansi Rani,"Ripple reduction using Butterworth LPF for Sensorless BLDC Motor Drive"International Journal of Advanced Research in Electrical, Electronics and Instrumentation Engineering,Vol. 3, Issue 4, April 2014.
[4] M. C. Chou, C. M. Liaw, S. B. Chien, F. H. Shieh, J. R. Tsai, and H.C. Chang, "Robust current and torque controls for PMSM driven satellite reaction wheel," IEEE Trans. Aerosp. Electron. Syst., vol. 47, no. 1,pp. 58–74, Jan. 2011.
[5] Y. S. Lai and Y. K. Lin, "A unified approach to zero-crossing point detection of back EMF for brushless DC motor drives without current and hall sensors," IEEE Trans. Power Electron., vol. 26, no. 6, pp. 1704–1713,Jun. 2011.
[6] R. J. Wang, M. J. Kamper, K. V. Westhuizen, and J. F. Gieras, "Optimal design of a coreless stator axial flux permanent-magnet generator," IEEE Trans. Magn., vol. 41, no. 1, pp. 55–64, Jan. 2005.
[7] M. Ooshima, S. Kitazawa, A. Chiba, T. Fukao, and D. G. Dorrell, "Design and analyses of a coreless-stator-type bearingless motor/generator for clean energy generation and storage systems," IEEE Trans. Magn.,vol. 42, no. 10, pp. 3461–3463, Oct. 2006.
[8] C. C. Hwang, P. L. Li, F. C. Chuang, C. T. Liu, and K. H. Huang, "Optimization for reduction of torque ripple in an axial flux permanent magnet machine," IEEE Trans. Magn., vol. 45, no. 3, pp. 1760–1763, Mar. 2009.
[9] S. J. Park, H.W. Park,M. H. Lee, and F. Harashima, "A new approach for minimum-torque-ripple maximum-efficiency control of BLDC motor,"IEEE Trans. Ind. Electron., vol. 47, no. 1, pp. 109–114, Feb. 2000.
[10] P. Mattavelli, L. Tubiana, and M. Zigliotto, "Torque-ripple reduction in PM synchronous motor drives using repetitive current control," IEEE Trans. Power Electron., vol. 20, no. 6, pp. 1423–1431, Nov. 2005.
[11] F. Aghili, "Adaptive reshaping of excitation currents for accurate torque control of brushless motors," IEEE Trans. Contr. Syst. Technol., vol. 16,no. 2, pp. 356–364, Mar. 2008.
[12] T. Kim, H. W. Lee, L. Parsa, and M. Ehsani, "Optimal power and torque control of a brushless DC (BLDC) motor-generator drive in electric and hybrid electric vehicles," Proc. Conf. Rec. IEEE IAS Annu. Meeting,pp. 1276–1281, Oct. 2006.
[13] Y. Liu, Z. Q. Zhu, and D. Howe, "Direct torque control of brushless DC drives with reduced torque ripple," IEEE Trans. Ind. Appl., vol. 41, no. 2,pp. 599–608, Mar./Apr. 2005.